Journal of Advanced Ceramics
2014, 3(2): 109–116
DOI: 10.1007/s40145-014-0099-8

ISSN 2226-4108
CN 10-1154/TQ

Research Article

Structural, optical and mechanical properties of ternary $CaO–CaF_2–P_2O_5$ glasses

G. VENKATESWARA RAO*, H. D. SHASHIKALA

Department of Physics, *National Institute of Technology Karnataka*, *Surathkal*, *Post Srinivasanagar*, *Mangalore-575025*, *Karnataka*, *India*

Received: January 07, 2014; Revised: February 20, 2014; Accepted: February 28, 2014

Abstract: The ternary phosphate glass series $(50–x)CaO–xCaF_2–50P_2O_5$ (x = 0–20 mol%) were synthesized using melt quench technique. Structural, optical and mechanical properties were investigated with increase in CaF_2 content. Using X-ray diffraction (XRD), synthesized glasses were confirmed to be amorphous in nature. Replacement of oxygen ions by fluorine ions increased the values of density. Decrease in refractive index due to the low polarizability of fluorine ions in the glass matrix was observed. In Fourier transform infrared (FTIR) spectra, the slight variation in ν_{as} (PO_2) band position and intensity could be attributed to replacement of fluorine ions for oxygen ions in phosphate glass structure. These data were well supported by Raman spectra. Optical band gap energy increased from 3.44 eV to 3.64 eV with increase in CaF_2 content, and Urbach energy decreased suggesting that the fluorine ions reduced the tail energy states in the band gap compared to the oxygen ions. Mechanical parameters such as Vickers hardness, fracture toughness and brittleness were evaluated from the Vickers micro indentation measurements. Increase in Vickers hardness, decrease in fracture toughness and increase in brittleness were observed with increase in CaF_2 content.

Keywords: phosphate glass; Fourier transform infrared (FTIR) spectra; Raman spectra; mechanical properties

1 Introduction

Modern technological applications have stimulated much importance in the study of optically transparent materials. Materials which have a broader optical transmission range from visible (Vis) to infrared (IR) wavelength region, gain much interest in the field of telecommunication, remote sensing, wave guides, photonics and optoelectronics [1–4]. Compared to oxide based glasses, fluoride based glasses show additional advantages, such as high transparency from IR to ultraviolet (UV) region, low glass transition temperature, low linear and nonlinear refractive index, low phonon energies and their potential as hosts for active rare earth ions [5,6]. However, these fluoride based glasses have various regular features, such as the chemical reactivity of fluoride melts, devitrification tendency and responsiveness to water. In that sense, the combination of oxides and fluorides, particularly oxyfluorophosphate glasses, appears to be very interesting and attractive materials [7,8].

* Corresponding author.
E-mail: venkatajabili@gmail.com

Development of low melting point oxyfluorophosphate glasses with low glass transition temperature, high chemical durability and high mechanical strength requires knowledge of their molecular and structural chemistry which is also essential to design them for practical applications. Many investigators introduced fluorine in oxide based glasses and studied the nature of bonding with the network forming cations using X-ray photoelectron spectroscopy (XPS) and nuclear magnetic resonance (NMR) spectroscopy [9–13]. They suggested that fluorine ions in glass covalently bond with network forming cations for lower fluorine content and bond with calcium ions for higher fluorine content. Also, they found that increase in band gap is due to the decrease in the donation of electrons from oxygen ions to glass modifiers. Hager applied Makishima and Mackenzie's theory to calculate the elastic moduli of boron oxyfluoride glasses and found that the mechanical properties such as longitudinal modulus, Young's modulus, shear and bulk modulus increase with replacing PbO by PbF_2 due to significant modification of the boron coordination polyhedra in the glass matrix [14,15]. On the other hand, there are only a few studies about the effects of fluorine addition on the optical and mechanical properties of phosphate based glasses.

The objective of this study is to examine the influence of the replacement of oxygen ions by fluorine ions in $(50–x)CaO–xCaF_2–50P_2O_5$ glasses with x varying from 0 to 20 mol% using Fourier transform infrared (FTIR), Raman and UV–Vis spectroscopy, and mechanical properties by Vickers indentation technique. In addition to these studies, density, molar volume and refractive index measurements have also been done on these glasses.

2 Experimental procedure

Glasses were synthesized by the conventional melt quench method using high purity Alfa Aesar chemicals such as CaO (99.9%), CaF_2 (≥ 99%) and P_2O_5 (≥ 98%) as starting materials. A batch of 20 g was weighed, thoroughly mixed in an agate mortar, then transferred into a silica crucible and melted at 1200 ℃ for 1 h in a PID controlled muffle furnace. After retaining the melt at that temperature for 1 h, it was cast into copper plates at room temperature. The obtained glass samples were then annealed at 400 ℃ for 5 h to relieve residual stresses developed during glass quenching and then slowly cooled to room temperature. Glasses were ground and polished on both sides to achieve a flat, optical quality surface for optical and mechanical measurements. The batch compositions of the studied glasses are shown in Table 1.

The X-ray diffraction (XRD) studies of the prepared glass samples were carried out using JEOL, JDX-8P X-ray diffractometer with Cu Kα radiation in the diffraction angle (2θ) range of 20°–80°. The X-ray tube was operated at 40 kV and 30 mA. The density of the glass samples was determined using the standard Archimedes method with xylene as the immersion fluid. The molar volume (V_m) was calculated using the formula $V_m = M/d$, where M is the glass molecular weight calculated from the batch composition and d is the measured density of the glass. The values of refractive indices were measured at room temperature using an Abbe refractometer (MAR-33) with an accuracy of ±0.001. The structural investigation was performed using FTIR spectrometer (JASCO-4200, Japan) within 400–4000 cm^{-1} at an average resolution of 32 scans per cm^{-1}. Raman spectra were also collected for all the glass samples using Alpha 300 WITec spectrometer with a spectral resolution of about 1 cm^{-1}. The optical absorption spectra were recorded using fibre optic spectrometer (SD 2000, Ocean Optics Inc., USA) in a spectral range from 250 nm to 850 nm. The Vickers hardness of the glasses was measured using Vickers diamond pyramid indentation technique (Clemex micro hardness tester, MMT X7, Matsuzawa Seiki Corp., Japan) by applying 0.98 N for 10 s.

Table 1 Batch composition and physical and optical properties of $(50–x)CaO–xCaF_2–50P_2O_5$ glasses

Sample	CaO (mol%)	CaF_2 (mol%)	P_2O_5 (mol%)	Density (±0.001 g/cm^3)	Molar volume (±0.01 cm^3/mol)	Refractive index (±0.001)	Optical band gap energy (eV)	Urbach energy (eV)
CPF0	50	0	50	2.589	38.24	1.547	3.44	0.390
CPF1	45	5	50	2.599	38.50	1.543	3.47	0.374
CPF2	40	10	50	2.612	38.74	1.540	3.53	0.371
CPF3	35	15	50	2.628	38.91	1.538	3.59	0.345
CPF4	30	20	50	2.637	39.20	1.534	3.64	0.314

Average hardness of ten indentations was taken for each glass specimen. For the fracture toughness measurements, indentations were performed on glass samples at 19.6 N to obtain median-radial cracks. The developed crack length measurement was done using optical microscopy. The indentations with median-radial cracks were further examined under scanning electron microscope (SEM, JEOL-JSM-6380LA, Japan). The glass samples were gold sputtered by using a JFC 1600 autofine coater (JEOL, Japan) before being observed under the SEM. Energy dispersive X-ray spectroscopy (EDX) was used to analyze the composition of glasses.

3 Results and discussion

The XRD patterns of the prepared glasses are shown in Fig. 1. No sharp diffraction peak can be observed in the spectra, which shows that the samples are indeed amorphous in nature. Table 1 shows the variation in density and molar volume of the studied glasses with the composition. The density of the glasses varies between 2.589 g/cm^3 and 2.637 g/cm^3 and is found to increase slightly with increase in CaF_2 content in the glasses. Since the ionic bonds are non-directional in nature, increasing the CaF_2 content will lead to the breakdown of the structural skeleton into a closer packing [15]. This leads to increase in measured density of the glasses. On the other hand, the values of molar volume V_m increase slightly from 38.24 cm^3/mol to 39.20 cm^3/mol with increase in CaF_2 content. Here CaF_2 acts as network modifier and introduces excess structural volume due to decrease in CaO content which leads to increase in the overall molar volume of the present glasses.

The addition of CaF_2 to the phosphate glasses leads to the decrease in refractive index from 1.547 to 1.534 by substituting oxygen ions with fluorine ions, which may be due to the smaller polarizability of fluorine ions than that of oxygen ions [16]. The batch composition of the prepared glasses and the values of density, molar volume and refractive index are summarized in Table 1.

Figure 2 shows the typical FTIR spectra in the wave number range from 400 cm^{-1} to 1600 cm^{-1} of (50–x)CaO–$x$$CaF_2$–50$P_2O_5$ glasses. As seen from this figure, the band at about 1287–1300 cm^{-1} is assigned to asymmetric stretching modes $\nu_{as}(PO_2)$ of the two

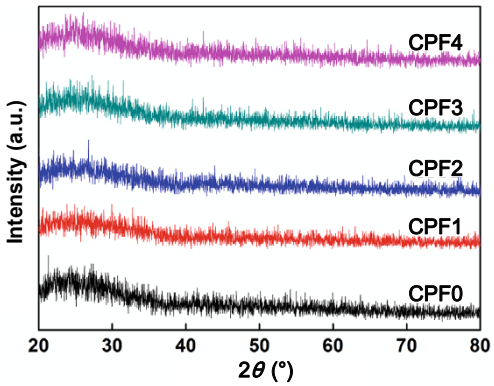

Fig. 1 XRD patterns of (50–x)CaO–$x$$CaF_2$–50 P_2O_5 glasses.

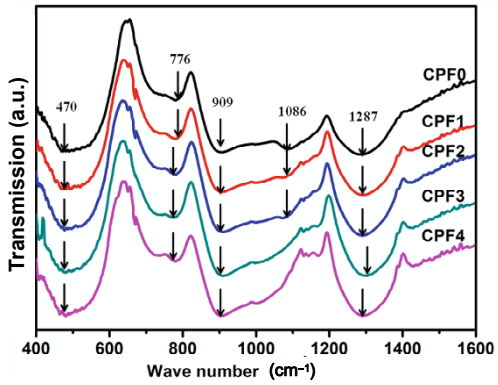

Fig. 2 FTIR spectra of (50–x)CaO–$x$$CaF_2$–50$P_2O_5$ glasses.

non-bridging oxygen atoms bonded to a phosphorus atom in the Q^2 phosphate tetrahedron. The intensity of $\nu_{as}(PO_2)$ band increases with increase in CaF_2 content. This may be due to the replacement of fluorine ions for oxygen ions at the constant P_2O_5 content leading to the increase in bond strength. Similarly, the asymmetric stretching of PO_3 group is present at around 1075–1086 cm^{-1} and is shifting to lower wave number. The intensity of these bands decreases up to 10 mol% CaF_2 and finally disappears. The absorption bands ν_{as} (P–O–P) and ν_s (P–O–P) occurring at about 906–910 cm^{-1} and 776–781 cm^{-1} are assigned, respectively to the asymmetric and symmetric stretching modes of the bridging oxygen atoms bonded to a phosphorus atom in the Q^2 phosphate tetrahedron. The slight variation in the band position is observed. The bands at around 470–480 cm^{-1} can be ascribed to deformation modes of PO_4^{3-} groups. The replacement of fluorine ions for oxygen ions at the constant P_2O_5 content does not disrupt the phosphate structure

drastically and the band assignments shown in Fig. 2 are consistent with the reported literature [13]. The corresponding band assignments for all the prepared glasses are summarized in Table 2.

Typical Raman spectra in the frequency range between 400 cm^{-1} and 1600 cm^{-1} of (50–*x*)CaO–*x*CaF_2–50P_2O_5 glasses are shown in Fig. 3. The spectra of all the prepared glasses exhibit similar spectral feature. As per the reported literature [9], the bands around 1278 cm^{-1} and 1174 cm^{-1} are due to asymmetric and symmetric stretching modes of out-of-chain PO_2 stretching respectively in the Q^2 phosphate tetrahedra. The absorption band around 700 cm^{-1} corresponds to the symmetric stretching modes of in-chain P–O–P of the bridging oxygen atoms bonded to two phosphorus atoms in Q^2 phosphate tetrahedra. As shown in Fig. 3, no new band is observed by replacing fluorine ions for oxygen ions. With increase of fluorine content, the intensity of about 1278 cm^{-1} band gradually increases due to the polymerization of the phosphate network [9]. Raman band assignments for all the prepared ternary calcium oxyfluorophosphate glasses are summarized in Table 3.

Tauc plots for ternary oxyfluorophosphate glasses are shown in Fig. 4. The absorption coefficient $\alpha(\omega)$ for the glasses can be associated with the optical band gap energy values by a power law proposed by Davis and Mott [17], which can be formulated as

$$\alpha(\omega) = B\frac{(\hbar\omega - E_{\text{opt}})^r}{\hbar\omega} \quad (1)$$

where $\alpha(\omega)$ is the absorption coefficient at an angular frequency, $\omega = 2\pi\nu$; B is a constant; E_{opt} is the optical band gap energy; $\hbar\omega$ is the photon energy of the incident beam; and index r can assume values of 1/2, 3/2, 2 and 3, depending on the mechanism of interband transitions. For the indirect transitions in glassy materials, the value $r = 2$ gives the best fit to the experimental results as suggested by Tauc [18] and Davis and Mott [17]. The values of optical band gap energy are obtained from extrapolation of the linear portion of the $(\alpha\hbar\omega)^{1/2}$ vs. $\hbar\omega$ plot and the intercept on the energy axis is shown in Fig. 4.

The absorption coefficient $\alpha(\omega)$ close to the band edge exhibits an exponential dependence on the incident photon energy $\hbar\omega$. The fundamental absorption edge generally obeys the Urbach rule [19]:

$$\alpha(\omega) = \alpha_0 \exp\left(\frac{\hbar\omega}{\Delta E}\right) \quad (2)$$

where α_0 is a constant; ΔE is the Urbach energy which shows the width of the band tails of the localized states within the energy gap. Urbach energy

Table 2 Infrared absorption bands for (50–*x*)CaO–*x*CaF_2–50P_2O_5 glasses

Infrared absorption band (cm^{-1})					Band assignment
CPF0	CPF1	CPF2	CPF3	CPF4	
470	472	478	478	480	Deformation modes of PO_4^{3-} groups
776	781	780	781	780	Symmetric stretch of P–O–P bridges
909	906	907	910	906	Asymmetric stretch of P–O–P bridges
1086	1075	1078	—	—	Asymmetric stretch of PO_3 groups
1287	1291	1293	1300	1291	Asymmetric stretch of PO_2 band

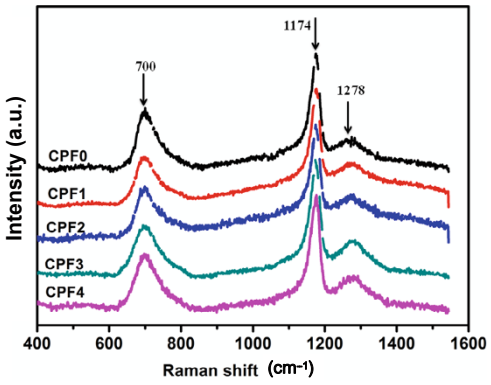

Fig. 3 Raman spectra of (50–*x*)CaO–*x*CaF_2–50P_2O_5 glasses.

Table 3 Raman bands for (50–*x*)CaO–*x*CaF_2–50P_2O_5 glasses

Raman band (cm^{-1})					Band assignment
CPF0	CPF1	CPF2	CPF3	CPF4	
700	699	701	695	696	Symmetric stretching modes of in-chain P–O–P of the bridging oxygen atoms
1174	1175	1175	1173	1175	Symmetric stretching modes ν_s (PO_2) of non-bridging oxygen atoms
1278	1276	1276	1274	1276	Asymmetric stretch of the ν_{as} (PO_2) of non-bridging oxygen atoms

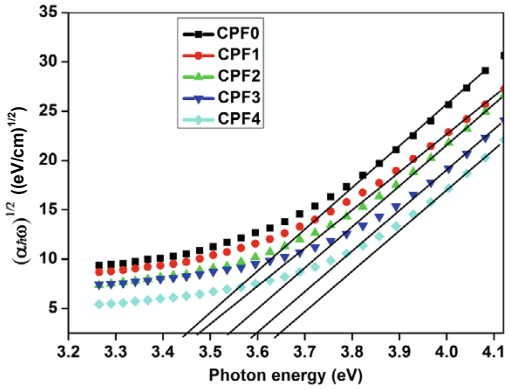

Fig. 4 Tauc plots of (50–x)CaO–$x$$CaF_2$–50$P_2O_5$ glasses.

is determined experimentally from the reciprocal of the slope of the linear portion of the $\ln\alpha$ vs. $\hbar\omega$ curves shown in Fig. 5 in the lower photon energy regions and is included in Table 1.

In the present investigation, the increase of E_{opt} from 3.44 eV to 3.64 eV with increase in CaF_2 content is probably related to the formation of non-bridging fluorine (NBF) atoms which are substituting the bridging oxygen (BO) atoms [20,21]. The optical band gap energy E_{opt} of these glasses depends on the surrounding metal ions and the concentration of bridging and non-bridging oxygen atoms. The optical transitions in these glasses are emerging from the excitation of electrons from the oxygen atom energy levels to the energy levels of the metal ions. The existence of negative charge on the non-bridging oxygen atoms assists the excitation of their electrons to the higher energy level. This mechanism is dominant in non-bridging oxygen in comparison with that of the bridging oxygen in which there is an absence of negative charge. In general, the electronegativity of fluorine atoms (3.98) is larger compared to that of oxygen atoms (3.44). The replacement of fluorine ions for oxygen ions causes decrease in the contribution of electrons from nearby ions and an increase in the average number of bridging oxygen atoms in the phosphate glass network because fluorine stabilizes more electrons than oxygen atoms causing increase in the optical band gap energy. A similar increase in E_{opt} values with an increase in non-bridging fluorine atom content has been reported for phosphate glasses [12]. In the present work, Urbach energy decreases from 0.390 eV to 0.314 eV as present in Table 1. The origin of Urbach energy in amorphous materials may be the stronger broadening of absorption edge compared with crystals. This origin can be attributed to the lack of long range order, density fluctuations, phonon-assisted indirect electron transitions and charged impurities [22].

Table 4 summarizes the mechanical properties of glasses analyzed in the present study. The mean value of Vickers hardness increases from 3.59 GPa to 3.89 GPa. Vickers hardness and Young's modulus are material properties. It is well known that elastic properties together with physical properties depend on the forces between atoms in the solid. Makishima and Mackenzie [23] proposed suitable model to evaluate the elastic properties of the glass packing density and the dissociation energies of the oxide constituents. The increase in Vickers hardness with increase in CaF_2 content may be due to the replacement of oxygen ions by fluorine ions in the glass matrix. The replacement causes the structure to be more compact and increases the cross linking strength [24]. In the present study, the Young's modulus (E) of the polycomponent glasses has been calculated using the theoretical equation proposed by Makishima and Mackenzie. Recently, Inaba *et al*. [25] has calculated the Young's modulus of several oxide based glasses and modified the dissociation energy of P_2O_5 from 62.8 kJ/cm^3 to 28.2 kJ/cm^3 in comparison with the values proposed by Makishima and Mackenzie. They found that a double bond (P=O) is a non-bridging bond and it does not contribute to the stiffness [26]. For the fracture toughness measurements, indentations were performed on glass samples at 19.6 N to obtain median-radial cracks. The developed median-radial crack length was measured using optical microscope. The fracture toughness was calculated, using the model proposed by Anstis *et al*. [27], which

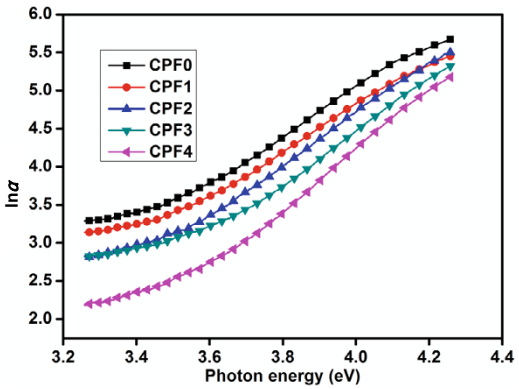

Fig. 5 $\ln\alpha$ as functions of photon energy for (50–x)CaO–$x$$CaF_2$–50$P_2O_5$ glasses.

Table 4 Vickers hardness, fracture toughness and brittleness values of (50–*x*)CaO–*x*CaF_2–50P_2O_5 glasses

Sample	Vickers hardness (GPa)	Measured half of the crack length (μm)	Fracture toughness (MPa·$m^{1/2}$)	Index of Brittleness ($\mu m^{-1/2}$)
CPF0	3.59	163	0.58	6.16
CPF1	3.65	170	0.54	6.72
CPF2	3.74	175	0.51	7.27
CPF3	3.81	182	0.48	7.91
CPF4	3.89	185	0.46	8.36

is given by

$$K_{IC} = 0.016\left(\frac{E}{H_V}\right)^{1/2}\left(\frac{P}{C^{3/2}}\right) \quad (3)$$

where E, H_V, C and P are Young's modulus (GPa), Vickers hardness (GPa), half of the crack length (μm) and applied load (19.6 N), respectively. Lawn and Marshall [28] have proposed a helpful model for the calculation of brittleness of glass, in which, index of brittleness B can be derived in terms of Vickers hardness and fracture toughness as

$$B = \frac{H_V}{K_{IC}} \quad (4)$$

where K_{IC} is the fracture toughness (MPa·$m^{1/2}$). The increase in brittleness from 6.16 $\mu m^{-1/2}$ to 8.36 $\mu m^{-1/2}$ with increase in CaF_2 content can be due to the lack of plastic flow, and the morphology obtained in the indentation pattern due to cracking as shown in SEM images of CPF4 supports this view [29]. Fracture toughness decreases and brittleness increases with increase in CaF_2 content and the values are given in Table 4. A typical SEM Vickers indentation and associated fracture pattern initiated for the 19.6 N crack initiation tests from the glass samples CPF0 and CPF4 are shown in Fig. 6.

Radial crack patterns generated by Vickers indentations are extensively used to determine the fracture toughness (K_{IC}) of glasses. Vickers diamond pyramidal indenter generates palmqvist cracks or median-radial cracks on the glass surface. In general, the cracks formed in all samples are originated from the four corners of the Vickers indentation, which often originates from the flaws and extends when the applied stress exceeds particular threshold. Table 4 shows decrease in the fracture toughness from 0.58 MPa·$m^{1/2}$ to 0.46 MPa·$m^{1/2}$ with increase in CaF_2 content, which is due to the increase in Young's modulus and crack length. Figure 6(a) is the SEM image of median-radial cracks generated by the application of 19.6 N indentation load on glass CFP0 made with Vickers indenter. An arrow mark indicates the median-radial cracks extending from the four corners of the Vickers indentation pattern. Figure 6(b) illustrates an indentation site in CPF4 glass. The bottom left crack appears as a lateral crack extending from the outer

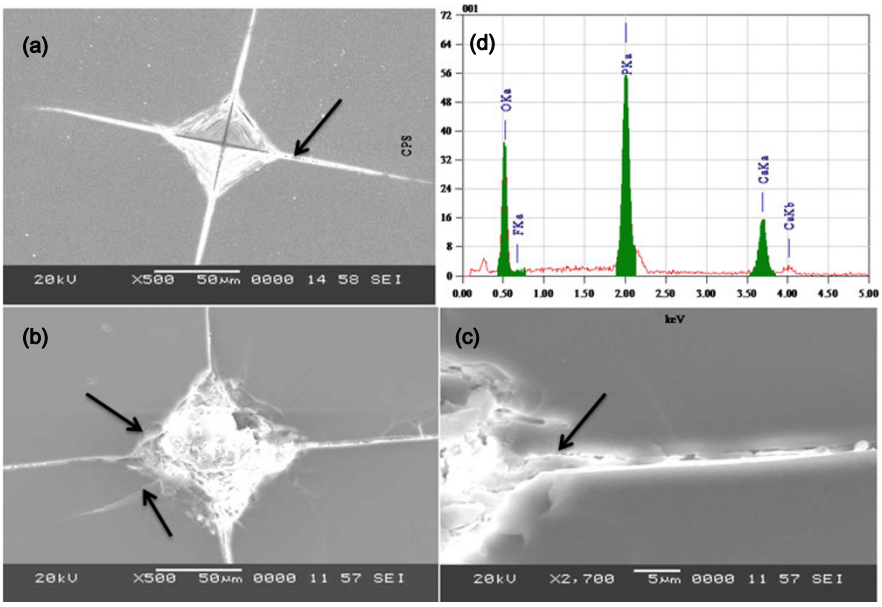

Fig. 6 SEM of Vickers impression with radial cracks of glass samples: (a) CPF0 and (b) CPF4; (c) magnified view of CPF4; (d) EDX of CPF4.

shear faults which is indicated by the solid arrow. Figure 6(c) is a higher magnified image of CPF4 glass. The white reflections of the bright region indicate that a large amount of surface chipping is apparent and shear cracks are also formed in the indentation print. This indicates the higher brittleness of CPF4 in comparison with CPF0. The solid arrow indicates that median-radial cracks are extending from the outer shear faults. Fracture toughness is a property concerned with the mean bond strength and it varies with Young's modulus. According to Osaka and Takahashi's results [30], the bond strength between the modifying cations and non-bridging oxygen is much weaker than that between the phosphorus and bridging oxygen or phosphorus and non-bridging oxygen. It was concluded that propagating cracks in these glasses may be due to the breakage of the weakest bonds between the non-bridging oxygen and the modifying cations. The EDX image of Fig. 6(d) shows that Ca, F, O and P elements are present in CPF4 glass.

4 Conclusions

Ternary oxyfluorophosphate glasses with the composition of $(50–x)CaO–xCaF_2–50P_2O_5$ ($x = 0$–20 mol%) were prepared by melt quench technique. Increasing the CaF_2 content gave rise to increase in both density and molar volume and decrease in refractive index. Optical absorption bands of both stretching and bending vibrations were obtained and analyzed using FTIR and Raman spectra. Increase in optical band gap energy and decrease in Urbach energy were observed with increase in CaF_2 content which may be due to the increase in average number of bridging oxygen. When the CaF_2 content was increased, the Vickers hardness increased, fracture toughness decreased while the brittleness increased. An increment in the brittleness of synthesized glass was further confirmed by SEM of median-radial cracks generated due to Vickers indentation. Presence of CaF_2 in the calcium phosphate glasses showed considerable effect on their mechanical and optical properties.

Acknowledgements

One of the authors GVR thanks National Institute of Technology Karnataka, Surathkal, for providing the institute fellowship. The authors thank Nano Functional Materials Technology Centre (NFMTC), Indian Institute of Technology Madras for carrying out Raman spectroscopy measurements.

References

[1] Ehrt D, Ebeling P, Natura U. UV transmission and radiation-induced defects in phosphate and fluoride–phosphate glasses. *J Non-Cryst Solids* 2000, **263–264**: 240–250.

[2] Stevenson AJ, Serier-Brault H, Gredin P, *et al*. Fluoride materials for optical applications: Single crystals, ceramics, glasses, and glass–ceramics. *J Fluorine Chem* 2011, **132**: 1165–1173.

[3] Sramek R, Fonteneau G, Josse E, *et al*. Planar and channel waveguides in fluoride glasses. *J Non-Cryst Solids* 1999, **256–257**: 189–193.

[4] Josse E, Fonteneau G, Lucas J. Low-phonon waveguides made by F^-/Cl^- exchange on fluoride glasses. *Mater Res Bull* 1997, **32**: 1139–1146.

[5] Adam J-L. Non-oxide glasses and their application in optics. *J Non-Cryst Solids* 2001, **287**: 401–404.

[6] Mortier M, Goldner P, Féron P, *et al*. New fluoride glasses for laser applications. *J Non-Cryst Solids* 2003, **326–327**: 505–509.

[7] Nazabal V, Poulain M, Olivier M, *et al*. Fluoride and oxyfluoride glasses for optical applications. *J Fluorine Chem* 2012, **134**: 18–23.

[8] Djouama T, Boutarfaia A, Poulain M. Fluorophosphate glasses containing manganese. *J Phys Chem Solids* 2008, **69**: 2756–2763.

[9] Tsunawaki Y. Analysis of $CaO–SiO_2$ and $CaO–SiO_2–CaF_2$ glasses by Raman spectroscopy. *J Non-Cryst Solids* 1981, **44**: 369–378.

[10] Osaka A, Wang YH, Miura Y, *et al*. X-ray photoelectron spectroscopy of lead fluorosilicate glasses. *J Mater Sci* 1991, **26**: 2778–2782.

[11] Hager IZ. Optical properties of lithium barium haloborate glasses. *J Phys Chem Solids* 2009, **70**: 210–217.

[12] Rao TGVM, Kumar AR, Reddy MR. Spectroscopic studies of tungsten ions in $PbO–PbF_2–SiO_2$ glasses. *J Non-Cryst Solids* 2012, **358**: 25–29.

[13] Iwamoto N, Makino Y. A structural investigation of calcium fluorosilcate glasses. *J Non-Cryst Solids*

1981, **46**: 81–94.
[14] Kurkjian CR. Mechanical properties of phosphate glasses. *J Non-Cryst Solids* 2000, **263–264**: 207–212.
[15] Hager IZ. Elastic moduli of boron oxyfluoride glasses: Experimental determinations and application of Makishima and Mackenzie's theory. *J Mater Sci* 2002, **37**: 1309–1313.
[16] Kitamura N, Fukumi K, Nakamura J, *et al*. Optical properties of fluorine-substituted zinc bismuth phosphate glasses. *J Non-Cryst Solids* 2011, **357**: 1188–1192.
[17] Davis EA, Mott NF. Conduction in non-crystalline systems V. Conductivity, optical absorption and photoconductivity in amorphous semiconductors. *Philos Mag* 1970, **28**: 903–922.
[18] Tauc J. States in the gap. *J Non-Cryst Solids* 1972, **8–10**: 569–585.
[19] Urbach F. The long-wavelength edge of photographic sensitivity and of the electronic absorption of solids. *Phys Rev* 1953, **92**: 1324.
[20] Kitamura N, Fukumi K, Nishii J, *et al*. UV absorption edge shift by doping alkali fluorides in fluoroaluminate glass. *J Phys Chem Solids* 2002, **63**: 691–694.
[21] Hill RG, Stamboulis A, Law RV. Characterization of fluorine containing glasses by ^{19}F, ^{27}Al, ^{29}Si and ^{31}P MAS-NMR spectroscopy. *J Dent* 2006, **34**: 525–532.
[22] Kranjčec M, Studenyak IP, Kurik MV. On the Urbach rule in non-crystalline solids. *J Non-Cryst Solids* 2009, **355**: 54–57.
[23] Makishima A, Mackenzie JD. Direct calculation of Young's modulus of glass. *J Non-Cryst Solids* 1973, **12**: 35–45.
[24] Yamane M, Mackenzie JD. Vicker's hardness of glass. *J Non-Cryst Solids* 1974, **15**: 153–164.
[25] Inaba S, Oda S, Morinaga K. Heat capacity of oxide glasses at high temperature region. *J Non-Cryst Solids* 2003, **325**: 258–266.
[26] Swarnakar AK, Stamboulis A, Holland D, *et al*. Improved prediction of Young's modulus of fluorine-containing glasses using MAS-NMR structural data. *J Am Ceram Soc* 2013, **96**: 1271–1277.
[27] Anstis GR, Chantikul P, Lawn BR, *et al*. A critical evaluation of indentation techniques for measuring fracture toughness: I, direct crack measurements. *J Am Ceram Soc* 1981, **64**: 533–538.
[28] Lawn BR, Marshall DB. Hardness, toughness and brittleness: An indentation analysis. *J Am Ceram Soc* 1979, **62**: 347–350.
[29] Sehgal J, Ito S. Brittleness of glass. *J Non-Cryst Solids* 1999, **253**: 126–132.
[30] Osaka A, Takahashi K. Heats of solution of the glasses and crystals in the systems $MO–P_2O_5$ and bond energy relations in $M(PO_3)_2$ glasses. *Yogyo Kyokai Shi* 1983, **91**: 394–398.